We are IntechOpen,
the world's leading publisher of
Open Access books
Built by scientists, for scientists

6,900
Open access books available

186,000
International authors and editors

200M
Downloads

154
Countries delivered to

Our authors are among the

TOP 1%
most cited scientists

12.2%
Contributors from top 500 universities

CLARIVATE ANALYTICS
BOOK CITATION INDEX INDEXED

WEB OF SCIENCE™

Selection of our books indexed in the Book Citation Index
in Web of Science™ Core Collection (BKCI)

Interested in publishing with us?
Contact book.department@intechopen.com

Hybrid Microstrip Antennas

Alexandre Perron, Tayeb A. Denidni and Abdel R. Sebak
Institut national de la recherche scientifique
Concordia University
Canada

1. Introduction

Various techniques can be used to increase the gain of an antenna. For example, two or more uniformly distributed radiating elements can be used to create an antenna array. Array antennas have been successfully used for several years, but, unfortunately, they still suffer from a fundamental disadvantage: their feeding structure is inevitably more complex and may generate considerable losses (Horng & Alexopoulos, 1993). This is especially true at millimeter-wave frequencies, where losses of 40% to 50% are not uncommon (Uchimura et al., 2005; Huang & Wang, 2006; Weily & Guo, 2009). This type of antenna is also somewhat limited by the mutual coupling of its individual elements (Mohammadian et al., 1989; Malherbe, 1989). These factors, combined with the greater quantity of materials required to manufacture an array, can be responsible for a longer time-to-market and higher production costs.

Nevertheless, array antennas can offer useful functionalities such as electronic beam steering, introduction of nulls in specific directions (to counter a source of interference, for example) and suppression of secondary lobes by adjusting the phase and/or amplitude of the signals feeding the individual elements. However, if these characteristics are not necessary for a given system, an array antenna might not be the best choice, especially if complexity and cost are issues.

The single element hybrid microstrip antennas presented in this chapter rely on a large electrical size to increase the gain. This is achieved by exciting a higher order mode inside a dielectric ring resonator. Two hybrid antennas that were designed and fabricated using this approach will be presented in this chapter. The first antenna is linearly polarized and the second has two orthogonal linear polarizations.

2. Linearly polarized hybrid microstrip antenna

2.1 Antenna configuration

Figure 1 shows the general shape of the first designed antenna. In essence, it is a hybrid antenna combining an aperture-fed circular microstrip patch with a ring-shaped dielectric resonator (DR). As opposed to other reported hybrid antennas (George et al., 1998; Esselle & Bird, 2005; Oh et al., 2007), the proposed antenna has a directive radiation pattern. Moreover, its design process is relatively straightforward, making it an interesting candidate for various commercial applications.

The DR ($\varepsilon_{r1} \approx 10$) is fed by a circular microstrip patch etched on a thin grounded dielectric layer with a low permittivity ($\varepsilon_{r2} \approx 2$). The patch itself is fed via a resonant slot in the ground
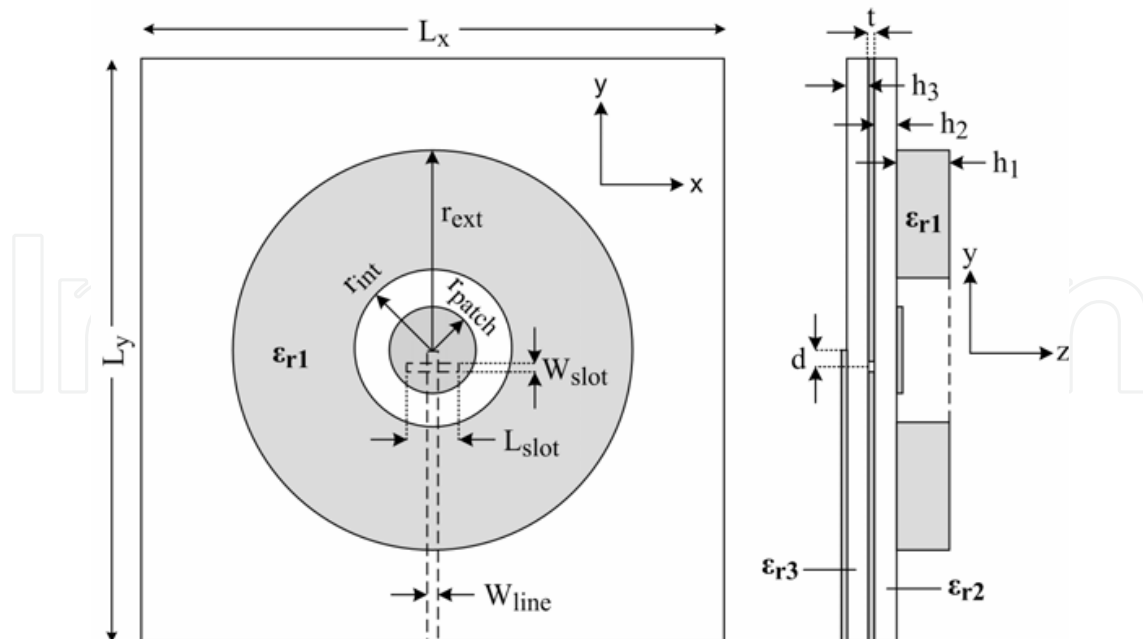
Fig. 1. Top and side views of the linearly polarized hybrid microstrip antenna

plane by a 50 Ω microstrip line sitting on the backside of a second thin dielectric layer with a higher permittivity ($\varepsilon_{r3} \approx 10$). The difference in permittivity ensures that the feed line is not as large as the patch ($W_{line} < 2\ r_{patch}$), a common problem encountered at millimeter-wave frequencies, where the physical dimensions of the conventional feeding structures are often comparable to those of the radiators.

2.2 Design procedure

The design process is relatively simple. The aperture coupled microstrip patch is first designed (without the DR) using conventional techniques - such as those described in this book - and its resonant frequency (TM_{110} mode) is adjusted so that the lower portion of the desired impedance bandwidth is covered. To reinforce the resonance, the length of the slot (L_{slot}) is approximately set to half a guided wavelength at a frequency just below the resonant frequency of the patch. During this first step, the width of the slot (W_{slot}) and other critical dimensions are chosen in function of the limitations of the PCB fabrication process. In our case, a minimum width of 0.1524 mm (6 mils) was tolerable.

For the DR, a $HEM_{1n\delta}$ (with n = 1, 3, 5 …) hybrid mode must first be selected and its resonant frequency is set so that the upper portion of the desired band is covered. We have found that the field configurations of this family of hybrid modes are well suited for coupling with a microstrip patch. However, care must be taken when choosing the order n of the hybrid mode as it has a direct effect on the shape of the far-field radiation pattern of the antenna. Fabrication constraints must also be considered.

Cohn's model (Cohn, 1968) is used to develop an estimation of the resonant frequency of the $HEM_{mn\delta}$ hybrid modes of a ring-shaped DR placed on a thin layer of grounded substrate:

$$f_{mn\delta}(GHz) = \frac{c}{2\pi\sqrt{\varepsilon_{eff}}}\sqrt{\left(\frac{\chi_{mn}}{r_{out}}\right)^2 + \left(\frac{\delta\pi}{2h_{eff}}\right)^2} \tag{1}$$

where c is the speed of light and χ_{mn} is the zero of derivative $J'_m(\chi_{mn}) = 0$ of the Bessel function $J_m(x)$ for odd values of n and the zero of $J_m(\chi_{mn}) = 0$ of the same Bessel function for even values of n. Table 1 lists the values of χ_{mn} for hybrid modes $HEM_{1n\delta}$ (n = 1 to 8).

Hybrid mode	χ_{mn}	Hybrid mode	χ_{mn}
$HEM_{11\delta}$	1.8412	$HEM_{15\delta}$	8.5363
$HEM_{12\delta}$	3.8318	$HEM_{16\delta}$	10.1735
$HEM_{13\delta}$	5.3315	$HEM_{17\delta}$	11.706
$HEM_{14\delta}$	7.0156	$HEM_{18\delta}$	13.3237

Table 1. Values of χ_{mn} for hybrid modes $HEM_{1n\delta}$ (n = 1 to 8)

The factor δ in Equation (1) is a quantity between 0 and 1 representing the number of half-wavelength variations of the field in the z direction. It can be calculated by solving the following set of equations:

$$\beta \cdot 2h_{eff} = 2 \cdot \tan^{-1}\left(\frac{\alpha}{\beta}\right) \tag{2}$$

$$\alpha = \sqrt{\left(\frac{\chi_{mn}}{r_{out}}\right)^2 - k_0^2} \tag{3}$$

$$\beta = \sqrt{k_0^2 \cdot \varepsilon_{eff} - \left(\frac{\chi_{mn}}{r_{out}}\right)^2} \tag{4}$$

$$\delta = \beta \cdot \frac{2h_{eff}}{\pi} \tag{5}$$

Equation (2) is transcendental in nature and can be easily solved numerically using a mathematical tool such as Matlab®. The effective height and the effective permittivity are defined as:

$$h_{eff} = h_1 + h_2 \tag{6}$$

$$\varepsilon_{eff} = \frac{V_{total}}{\dfrac{V_{hole}}{\varepsilon_{air}} + \dfrac{V_{ring}}{\varepsilon_{r1}} + \dfrac{V_{substrate}}{\varepsilon_{r2}}}$$
$$= \frac{r_{out}^2 \cdot h_{eff}}{\dfrac{r_{in}^2 \cdot h_1}{\varepsilon_{air}} + \dfrac{h_1(r_{out}^2 - r_{in}^2)}{\varepsilon_{r1}} + \dfrac{r_{out}^2 \cdot h_2}{\varepsilon_{r2}}} \tag{7}$$

where ε_{air} is the permittivity of air (≈ 1), V_{hole} is the volume of the DR hole, V_{ring} is the volume of the dielectric ring itself (without the hole), $V_{substrate}$ is the volume of the dielectric layer directly underneath the DR, and V_{total} is the sum of these three volumes.

2.3 Simulation results

Using the commercial electromagnetic simulator CST Microwave Studio®, the proposed antenna is simulated and optimized for operation in the 57 GHz to 65 GHz band. The final optimized values for the parameters of Figure 1 are listed in Table 2.

Parameter	Value (mm)	Parameter	Value (mm)
ε_{r1}	10.2	r_{ext}	3.6
ε_{r2}	2.2	r_{patch}	0.78
ε_{r3}	10.2	L_{slot}	0.835
h_1	0.635	W_{slot}	0.1524
h_2	0.254	d	0.2
h_3	0.254	L_x	10.5
r_{int}	1.3	L_y	10.5

Table 2. Parameter values (Figure 1) used for the simulations

Simulated S_{11} parameters of the aperture coupled microstrip antenna (without the DR) and of the proposed hybrid antenna (with the DR) are shown in Figure 2. The negative peak near 59 GHz (for both the microstrip and the hybrid antenna) is the result of the combination of
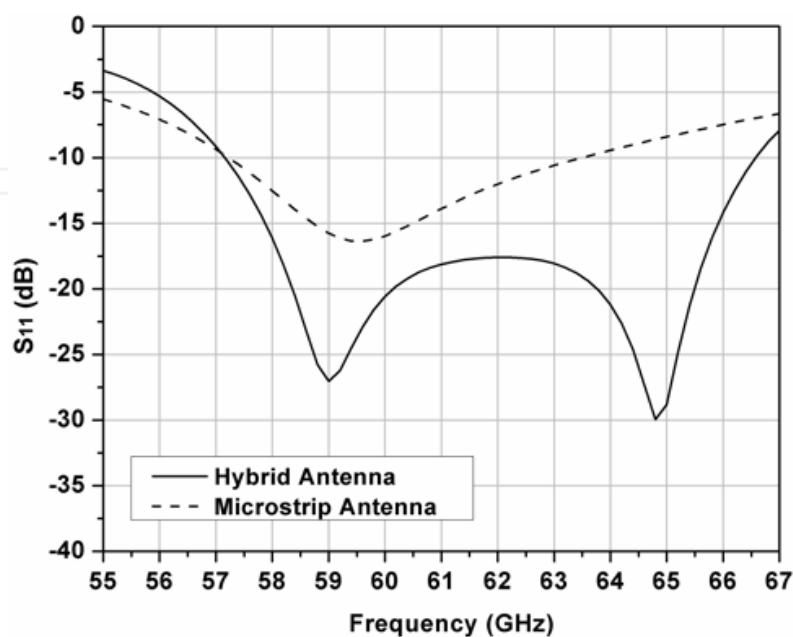

Fig. 2. Simulated S_{11} parameter of the linearly polarized hybrid antenna

two closely spaced resonances: one from the patch itself and another one from the resonant coupling slot. For the microstrip antenna (without the DR), the effect of this combination can be observed as the upper portion of the bandwidth of the patch is extended.

For the hybrid antenna, a second negative peak (near 65 GHz) is observed. It is the result of the excitation of the $HEM_{15\delta}$ hybrid mode inside the DR. Indeed, solving Equations (1) through (7), we find that h_{eff} = 0.889 mm, ε_{eff} = 3.522, δ = 0.6537, and $f_{15\delta}$ = 67.1 GHz (a difference of about 3%). For some designs, it may be possible to excite another mode within the $HEM_{1n\delta}$ (n = 1, 3, 5 …) family, given that the r_{out}/h_{eff} ratio and inner radius (r_{in}) of the DR are properly adjusted to maximize the coupling with its feeding structure. Generally, a ratio between 1 and 4 is expected for n = 1, 3, and 5, whereas modes with higher indices require a larger ratio, making the antenna too large for typical applications.

Three normalized radiation patterns at the lower edge, the center and the upper edge of the impedance bandwidth are shown in Figure 3. The first observation is that the main lobe is always directed at broadside and that secondary lobes are generated and get more visible as the frequency increases. These side lobes are a direct consequence of the excitation of the


57 GHz

61 GHz
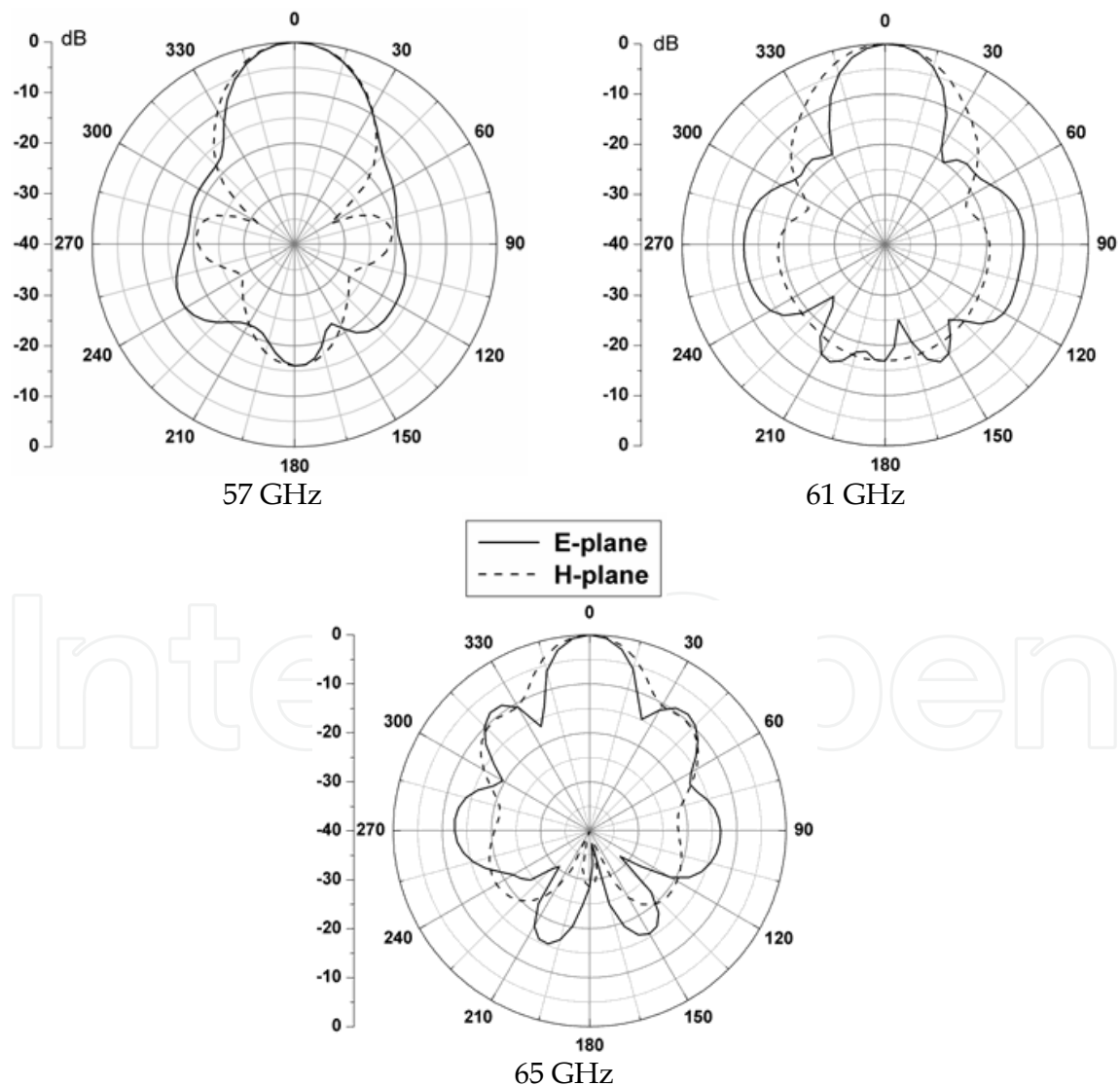
65 GHz

Fig. 3. Simulated radiation patterns of the linearly polarized hybrid antenna

HEM$_{15\delta}$ hybrid mode inside the DR. Nevertheless, they remain within acceptable levels, i.e. more than 9 dB lower than the main beam (at 65 GHz).

The half-power beamwidth is reduced as the frequency increases from 57 to 65 GHz (32.1° to 22.1° for the E-plane and 32° to 26° for the H-plane). However, this does not translate into a gain increase due to the increase in the side lobe levels. Another interesting quality of the proposed antenna is its very low cross polarization level, which is less than -27 dB (not shown).

The most appealing feature of this antenna resides in its high gain, as depicted in Figure 4. Indeed, it can be noted that the simulated gain is very high for such a simple structure i.e. more than 13 dB (with a simulated radiation efficiency between 86.8 and 89.7 % over the whole bandwidth). The gain is also stable over the bandwidth of interest, with a variation of about 0.35dB over the whole frequency band. The theoretical gain in Figure 4 is calculated with the following approximation formula (with a radiation efficiency η = 1 or 100%):

$$Gain(dB) = 10\log\left(\frac{\eta \cdot 4\pi \cdot A}{\lambda_0^2}\right) \tag{8}$$

where $A = \pi \, r_{out}^2$ is the physical area of the antenna and λ_0 is the free space wavelength. Since Equation (8) is only an approximation, it is not abnormal to see the simulated gain exceed the maximum theoretical value; this does not imply that the efficiency is over 100% for the lower portion of the bandwidth. Nonetheless, this theoretical approximation gives an upper limit for the gain we can expect from the proposed antenna.
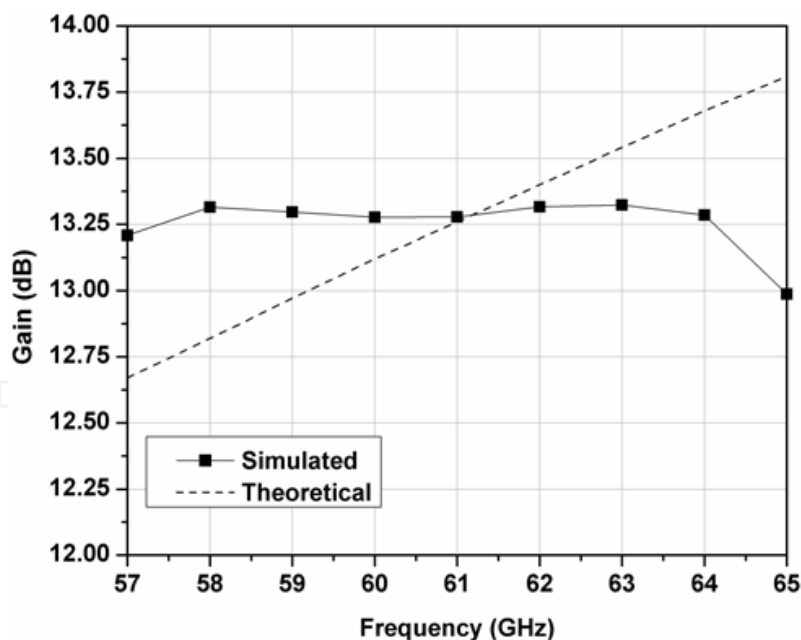

Fig. 4. Simulated gain of the linearly polarized hybrid antenna

2.4 Experimental results

A standard low cost PCB process is used to fabricate most of the antenna. Alignment holes are drilled outside the ground plane of the antenna to ensure that different components of the aperture coupled microstrip antenna are correctly aligned. The laminates are then

"glued" together using a thin film of bounding material and cut to the desired size, leaving out the alignment holes. The DR is cut using a computer controlled Nd-Yag Q-switched laser (a photograph of many fabricated samples is shown as an inset in Figure 5).

Figure 5 shows photographs of the fabricated antenna. The widely used RT/Duroid® 5880 is chosen as the substrate of the patch (ε_{r2} = 2.2, h_2 = 0.254 mm) whereas the feed line is etched on a thin layer of RT/Duroid® 6010LM (ε_{r2} = 10.2, h_3 = 0.254 mm).
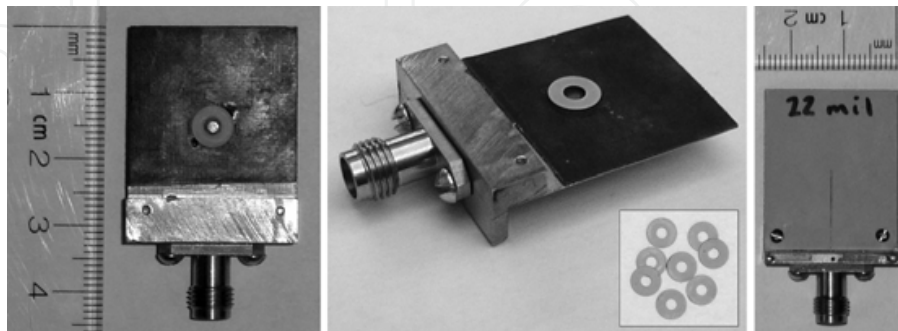
Fig. 5. Photographs of the linearly polarized hybrid microstrip antenna

All the dimensions are as listed in Table 2, except for L_x (25 mm), L_y (30 mm) and r_{out} = 3.2 mm. A larger ground plane was necessary to install the required housing to hold a 1.85 mm connector, for measurement purposes. A slightly smaller DR was chosen to suppress the undesired $HEM_{14\delta}$ hybrid mode, for which the calculated cutoff frequency fell too close to the operational band (56.7 GHz).

The S_{11} parameter of the prototype (with and without the DR) was measured using a Anritsu® 37397C Vector Network Analyzer (VNA). The results are presented in Figure 6.
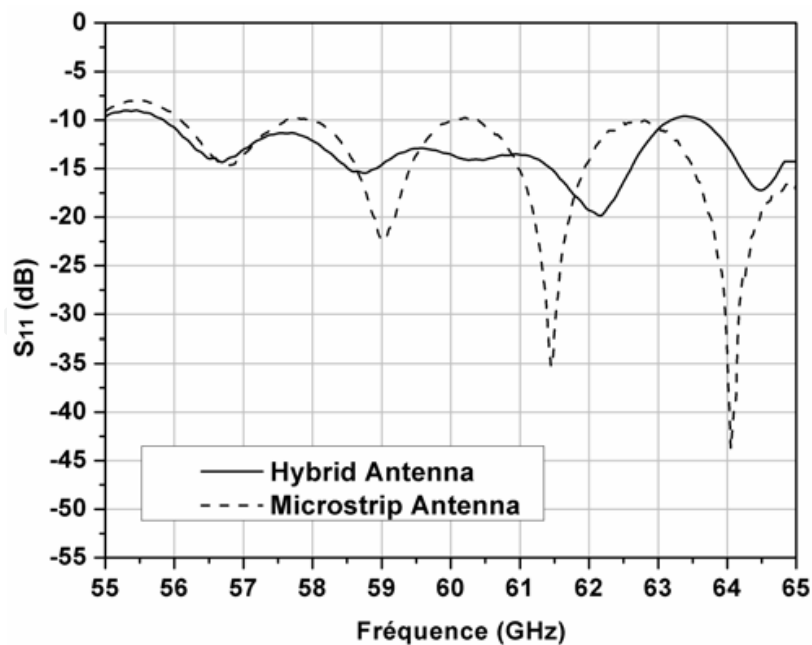

Fig. 6. Measured S_{11} of the microstrip (without the DR) and hybrid (with the DR) antennas

Considering the fact that the prototype is fabricated using a standard PCB process, that the two substrate layers are bounded together with a material of non-zero thickness, and that a connector is manually added, some discrepancies between the simulated and measured

results are expected. However, after a thorough investigation, it was found that the coaxial-to-microstrip transition (the connector) was responsible for the oscillations in the S_{11} curves.

A simple setup is used to measure the radiation patterns of the prototype. A standard gain V-band horn antenna (24 dB gain at mid-band) is connected to port 2 of the VNA and the antenna under test (AUT) is connected to port 1. Both antennas are vertically and horizontally aligned and are placed at a distance of 30 cm. The AUT is then manually rotated around its vertical axis by increments of 10-degrees and the S_{12} parameter is saved for post-processing. The measured H-plane normalized patterns (microstrip antenna and hybrid antenna) are plotted in Figure 7.

57 GHz   61 GHz

65 GHz
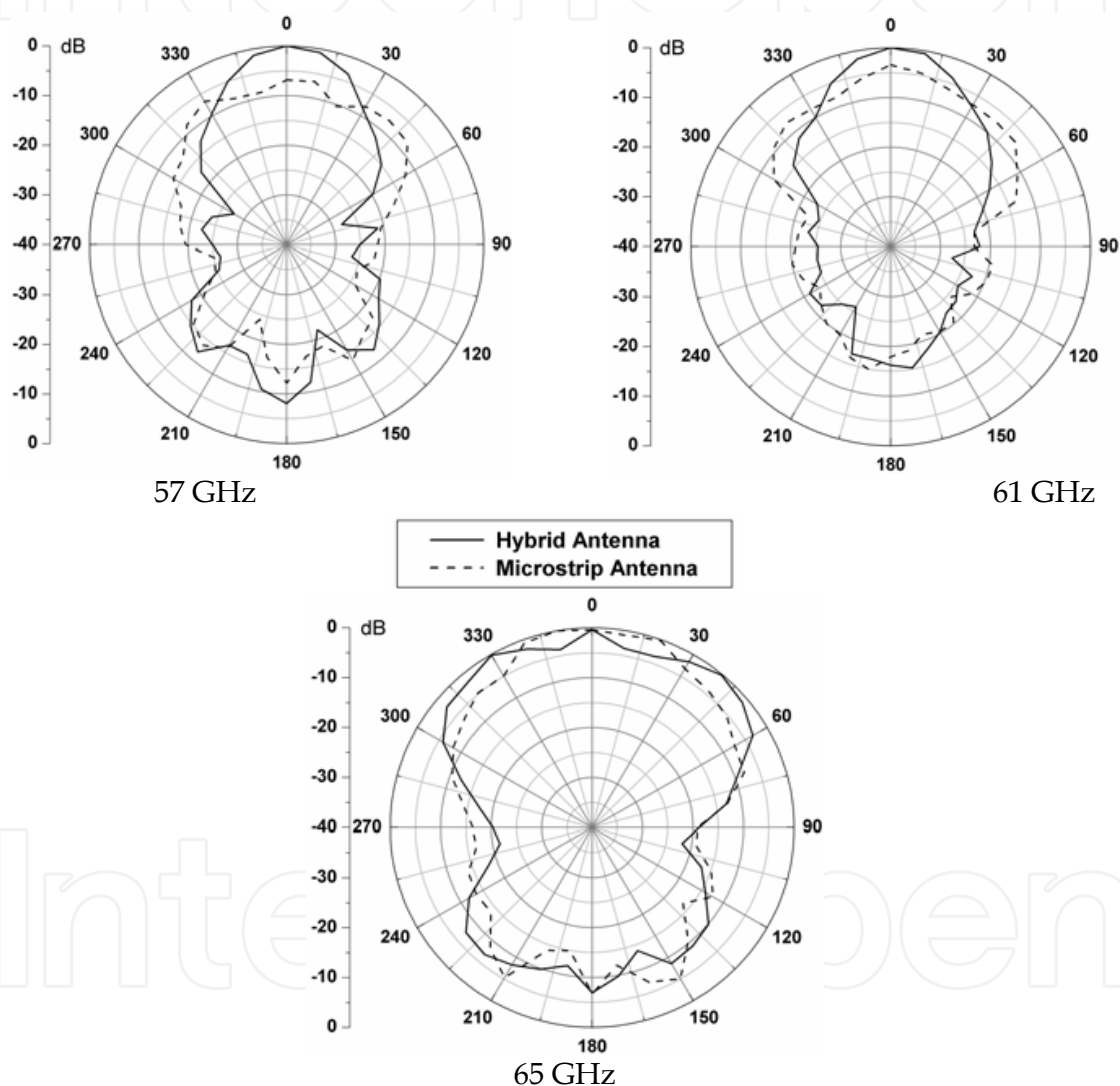
Fig. 7. Measured radiation patterns of the microstrip and hybrid microstrip antennas

The first observation we can make from these patterns is that, all things considered, the hybrid antenna is more directive than the aperture coupled microstrip antenna, except at the upper limit of the band (65 GHz), where the $HEM_{14\delta}$ mode manifestly takes over to generate a monopole-like pattern with a small peak at broadside. Secondly, the patterns of the hybrid antenna are stable over a large frequency range and are very similar to the simulated H-plane patterns presented as *dashed lines* in Figure 3. Indeed, the main lobe is dominant for

most of the bandwidth and the front-to-back ratio is between 10-15 dB. The backward radiation is higher than expected due to the strong resonance of the slot, especially near 57 and 65 GHz. Small side lobes at 90° and 270° can also be observed at some frequencies.

Using two identical standard gain horns, the gain is measured by applying the gain-transfer technique (Balanis, 2005) and removing the reflection losses with the aid of Figure 6. The measured results are presented in Figure 8. New simulated results taking into account the larger ground plane are plotted. The theoretical results are also recalculated based on the new outer radius of the DR (r_{out} = 3.2 mm).
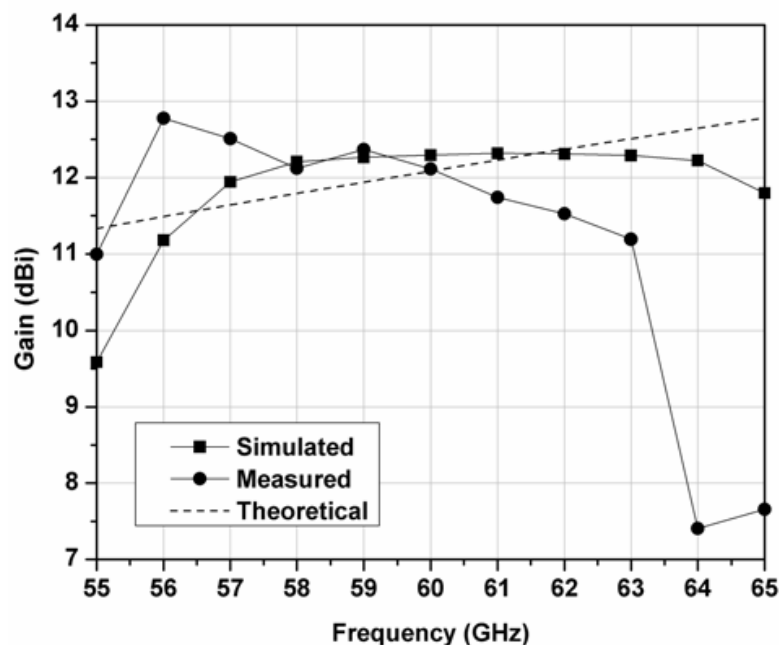
Fig. 8. Measured gain of the linearly polarized hybrid microstrip antenna

The measured gain is quite close to the simulated values. It is also stable over a large portion of the impedance bandwidth, as predicted. The theoretical gain is lower for r_{out} = 3.2 mm due to the reduced area occupied by the DR. Nonetheless, the measured gain is over 11 dB from 55 to 63 GHz, a bandwidth that would be large enough to cover the whole 57-65 GHz ISM band. The realized gain (not shown) is over 10.5 dB from 55 to 63 GHz.

2.5 Discussion

This section highlighted an innovative high-gain hybrid antenna for millimeter wave applications. A thorough theoretical study of the behavior of this antenna made it possible to define a simple design procedure. The proposed configuration achieves double digit gain by coupling a microstrip patch with a ring-shaped DR, thus increasing the electric size of the antenna. Indeed, simulated and measured results confirmed that the gain is clearly improved when the patch is correctly exciting an appropriate hybrid mode inside the dielectric structure. Furthermore, measurements from a prototype have also established that the major part of the antenna can be manufactured with a simple PCB process, that it is more directive than a conventional microstrip antenna, and that its impedance bandwidth would be large is enough to cover the whole ISM 57-65 GHz band.

3. Dual-polarized hybrid microstrip antenna

In this section another high gain and wide-band antenna designed from the same hybrid configuration will be presented. This second antenna could be used to transmit and/or receive signals by using two orthogonal linear polarizations (vertical and horizontal), via two independent feed ports.

3.1 Antenna configuration

The proposed antenna geometry is shown in Figure 9. A ring-shaped dielectric resonator (DR) ($\varepsilon_r = 10.2$; tan $\delta = 0.0023$) is fed by a square patch etched on a dielectric substrate (thickness = 0.254 mm; $\varepsilon_r = 2.2$; tan $\delta = 0.001$). The patch is fed via two orthogonally disposed slots of identical dimensions in the ground plane by two 50 Ω microstrip lines sitting on the backside of a second substrate layer (thickness = 0.254 mm; $\varepsilon_r = 10.2$; tan $\delta = 0.0023$).
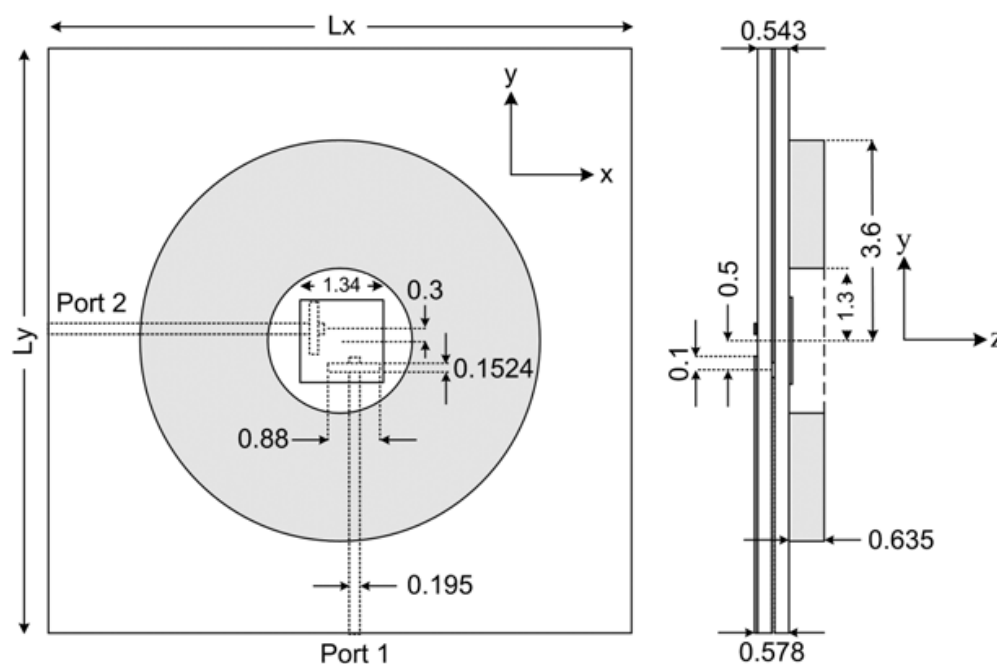
Fig. 9. Top and side views of a dual-polarized hybrid microstrip antenna

The L-shaped arrangement of the coupling slots ensures that both ports exhibit the same theoretical return loss, i.e. the same impedance bandwidth. A T-shaped disposition could be used to increase the isolation (Porter et al., 1999), but the impedance bandwidth of the two ports would then be dissimilar. The same observation has been made in (Perron et al., 2007) for a dual-polarized CPW-fed microstrip antenna operating at 2.45 GHz.

3.2 Results

A prototype of the proposed antenna was fabricated using Rogers Corporation® high frequency laminates (RT/Duroid® 5880 and 6010LM). The DR was easily cut using a computer controlled Nd-Yag Q-switched laser and bonded to the substrate with a few droplets of cyanoacrylate. Figure 10 shows photographs of the fabricated antenna. Again, note that a relatively large ground plane (Lx = Ly = 30 mm) is used to install a brass housing to hold two 1.85 mm connectors.
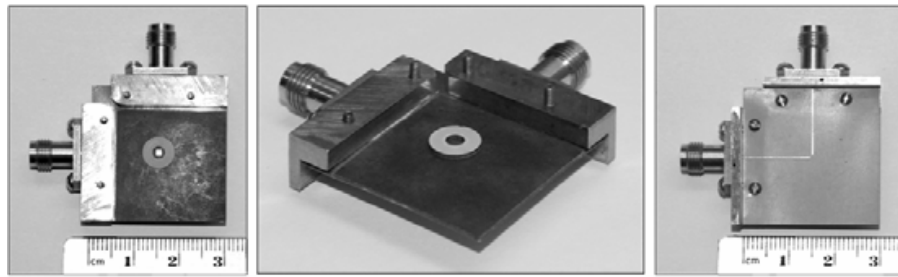
Fig. 10. Photographs of the dual-polarized hybrid microstrip antenna

The S-parameters of the antenna are measured using the VNA. The results are presented in Figure 11. For comparison, simulated results from CST Microwave Studio® are also plotted.
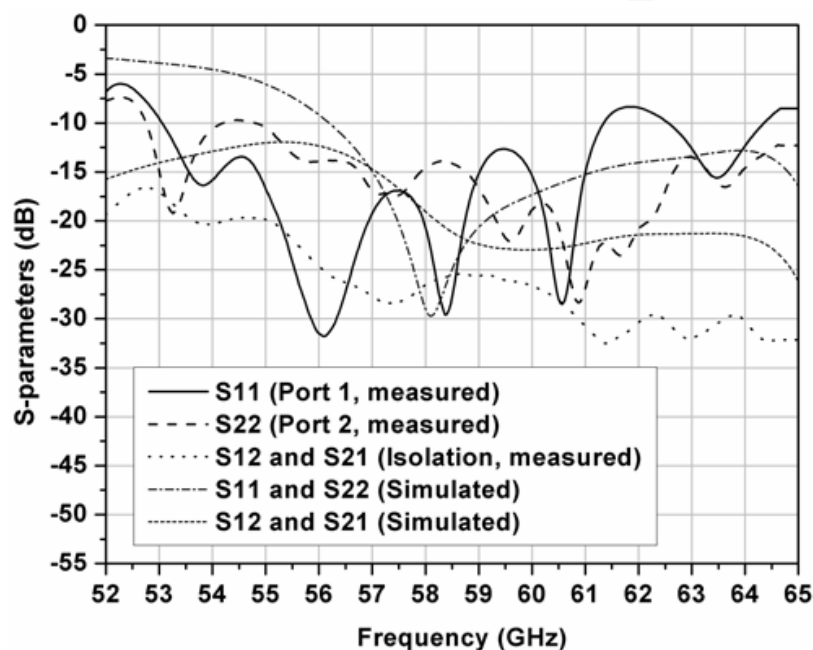

Fig. 11. Measured S-parameters of the dual-polarized hybrid microstrip antenna

Since the connectors and the brass support are not included in the simulation model (to decrease computational time), some discrepancies between measured and simulated data are expected. Nevertheless, the impedance bandwidth (VSWR < 2) of both ports of the antenna is fairly similar and is more than acceptable for many antenna applications. As the bandwidth is relatively large (more than 8 GHz), oscillations in the measured curves are also noticeable. This phenomenon is due to the inductive loading effect of the coaxial to microstrip transition. The measured isolation is better than expected, remaining over 20 dB over most of the bandwidth.

Using a three-antenna technique, the antenna gain for both polarizations is measured. Two result sets are presented in Figure 12: the gain of the antenna without the DR in place (the microstrip patch only) and the gain of the hybrid configuration (microstrip patch and DR). Alignment errors during the fabrication and variable transition losses introduced by the connectors are responsible for the differences between the two ports. Nevertheless, the hybrid configuration exhibits a higher gain, with a peak value of more than 10 dB at 56 GHz for both polarizations. The average simulated gain of the simplified model is 11.8 dB within the operational bandwidth of the antenna. This high-gain is due to the increase in the electrical size of the radiator when the DR is mounted on its surface.
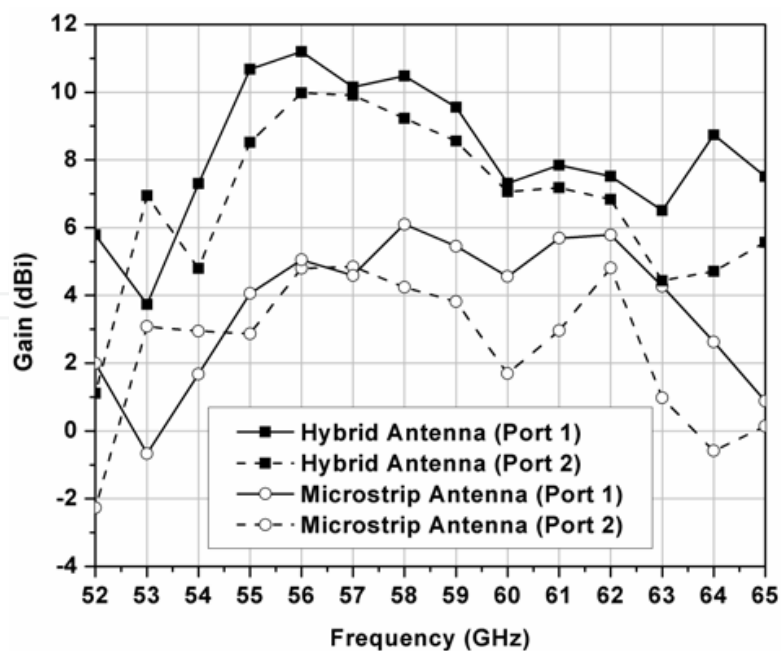
Fig. 12. Measured gain of the dual-polarized microstrip and hybrid configurations

The radiation pattern of the proposed antenna at 56 GHz (port 1) is presented in Figure 13. The pattern of port 2 (not shown) is almost identical. The patterns are measured manually using a simple yet precise mechanical setup covered with RF convoluted foam absorbers. A high-gain horn antenna is connected to the first port of the VNA while the second port is connected to the antenna under test. The S_{21} parameter at different angles is then stored for post-processing. Note that only half of the E-plane is measured since the connector would block the other half. For convenience, the other half is therefore estimated by mirroring the measured half. This is not the case for the H-plane which is completely measured. Again, the measured results incorporate both the microstrip patch and hybrid configurations.
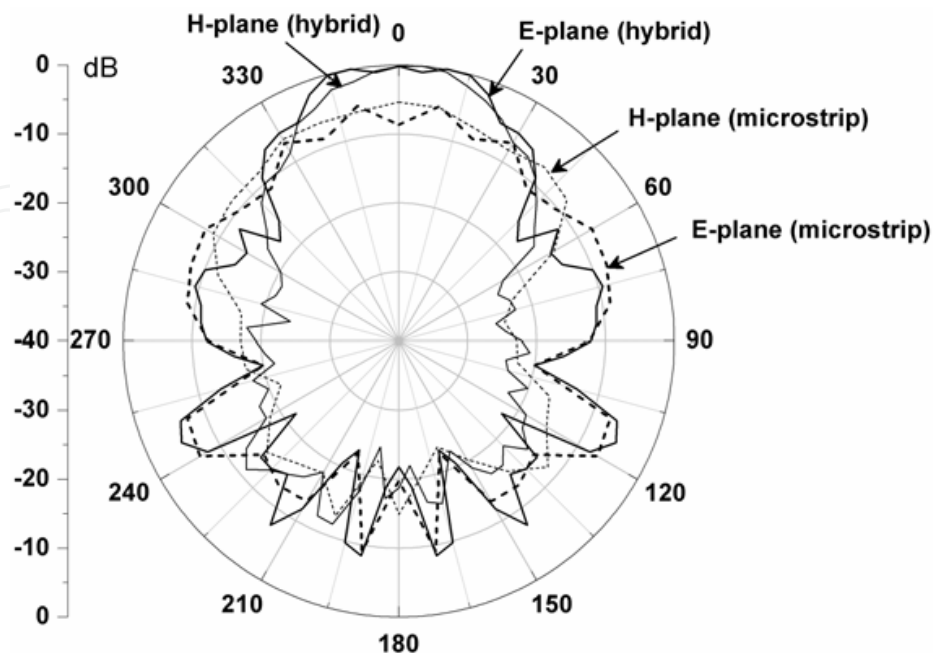

Fig. 13. Measured E- and H-plane of the microstrip and hybrid configurations (56 GHz)

The first observation is that the main beam of the antenna is directed at broadside and that the hybrid configuration is more directive than the microstrip patch antenna by itself. Also note the presence of small side lobes at 75° and 285° in the E-plane of the hybrid configuration. These side lobes are a result of the excitation of a higher order hybrid mode inside the DR (the $HEM_{13\delta}$ mode). In fact, by studying the electromagnetic distribution inside the ring-shaped DR, it can be seen that the latter acts as a dielectric waveguide that collects (or distributes) electromagnetic waves through a large aperture size. Unfortunately, as the frequency increases, the side lobes become more important and the gain decreases.

3.3 Discussion
A new hybrid microstrip antenna with two orthogonal linear polarizations has been presented in this section. Experimental results indicate that it could be used for applications requiring a high gain and a relatively broad bandwidth. Moreover, as this antenna is based on standard commercial components and that it is almost entirely manufactured with a conventional PCB process, it constitutes an interesting alternative to more complex configurations, such as array antennas. Finally, even if the prototype presented in this section exhibits a maximum gain at 56 GHz, it would undoubtedly be possible to optimize its dimensions so that the maximum gain is reached inside the 57-65 GHz band.

4. Possible improvements

The hybrid microstrip antennas presented in Sections 3 and 4 possess several desirable characteristics, making them excellent candidates for several millimeter-wave applications. In an effort to further improve their performance, a new modified geometry (with a higher gain and reduced side lobe levels) is presented in this section.

4.1 Antenna configuration
The modified configuration is presented in Figure 14. The dimensions of the radiating elements are the same as in Section 2. A brass support allows the antenna to be fitted with a 1.85 mm coaxial connector (note that the model in Figure 14 only shows the glass bead that is used to make the transition from the central conductor of the coaxial connector to the
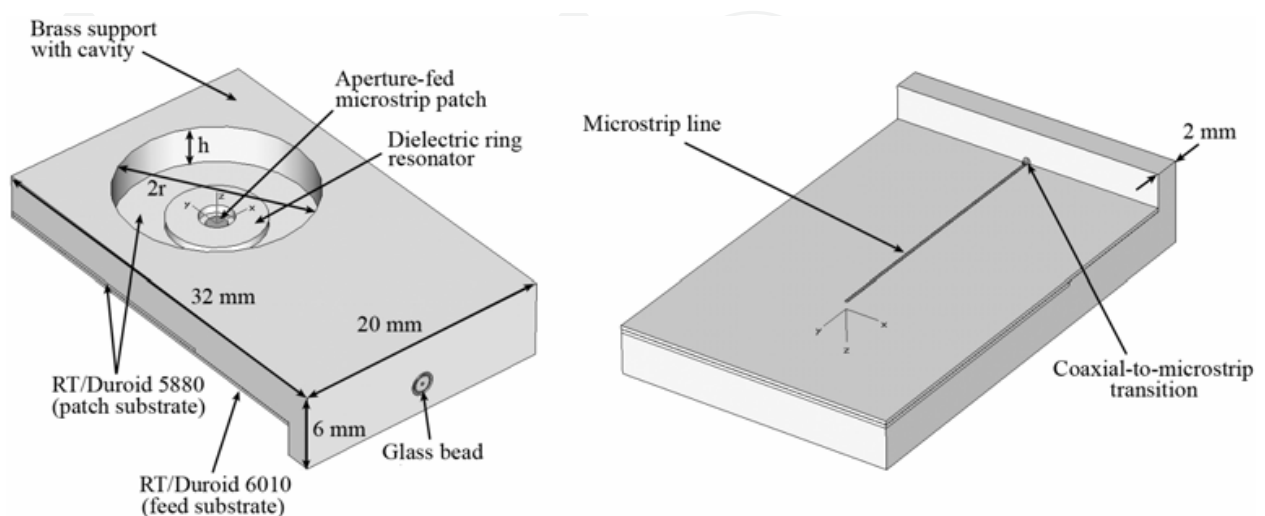

Fig. 14. Top and bottom views of the modified antenna geometry.

microstrip feed line). This housing adds a much needed structural support to the very thin PCB assembly. Indeed, both the feed substrate (RT/Duroid 6010, ε_r = 10.2) and the microstrip patch substrate (RT/Duroid 5880, ε_r = 2.2) are only 0.254 mm thick The brass support also features a circular opening (of height h and radius r) positioned directly above the DR and the patch. As it will be confirmed in the next section, it is possible to increase the gain and reduce the side lobe levels of the antenna by optimizing the dimensions of this metallic cavity.

4.2 Simulation results

In order to highlight the effects of adding a metallic cavity to the antenna, this section presents a number of antenna parameters simulated with and without the brass support (and cavity).

The simulated S_{11} of the proposed antenna (with and without the brass support) is shown in Figure 15. Note that the simulation port is located at the end of the microstrip feed line rather than at the end of the glass bead. This allows a better comparison of both antenna configurations and reduces computational time as the coaxial-to-microstrip transition is not unnecessarily simulated. The optimized dimensions of the cavity are h = 3 mm and r = 7.25 mm. In both cases, the impedance bandwidth (VSWR < 2) is wide, ranging from 56.5 to 66.5 GHz (16.3 %), approximately. The strongest resonances come from the patch and the DR, but the cavity itself affects the S_{11} parameter of the antenna by introducing small oscillations in the curve, especially at the upper end of the impedance bandwidth. By studying the input impedance of the antenna, we conclude that these oscillations are a result of a loading effect introduced by the brass support. Nonetheless, the reflection coefficients of both configurations are similar.
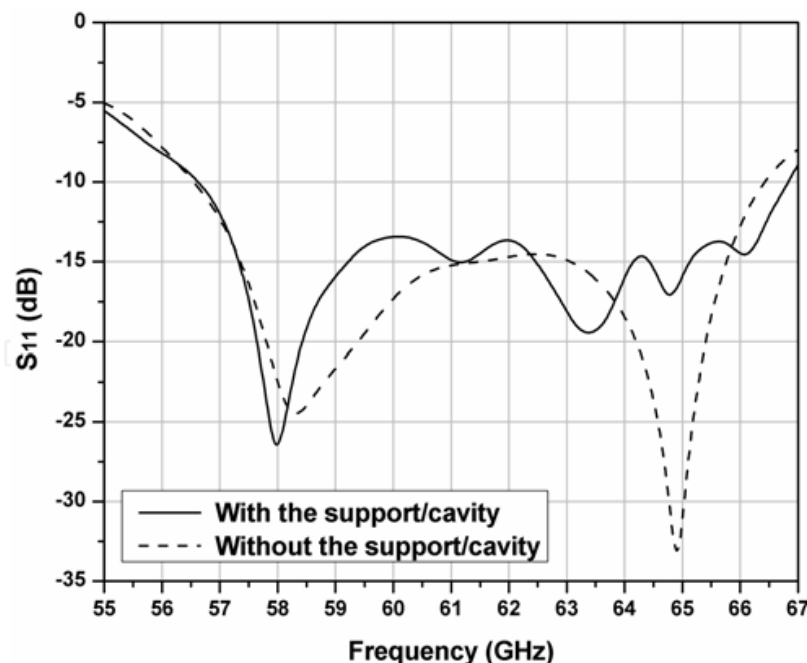

Fig. 15. Simulated S_{11} of the antenna (with and without the support and cavity).

Figure 16 and Figure 17 show the simulated gain and side lobe suppression levels of both configurations, respectively. From Figure 16, it is evident that the gain is improved when the support and cavity are present. This is most likely due to the constructive interference of

waves reflected by the wall of the latter. Figure 17 confirms that the side lobe suppression is better for most of the impedance bandwidth.
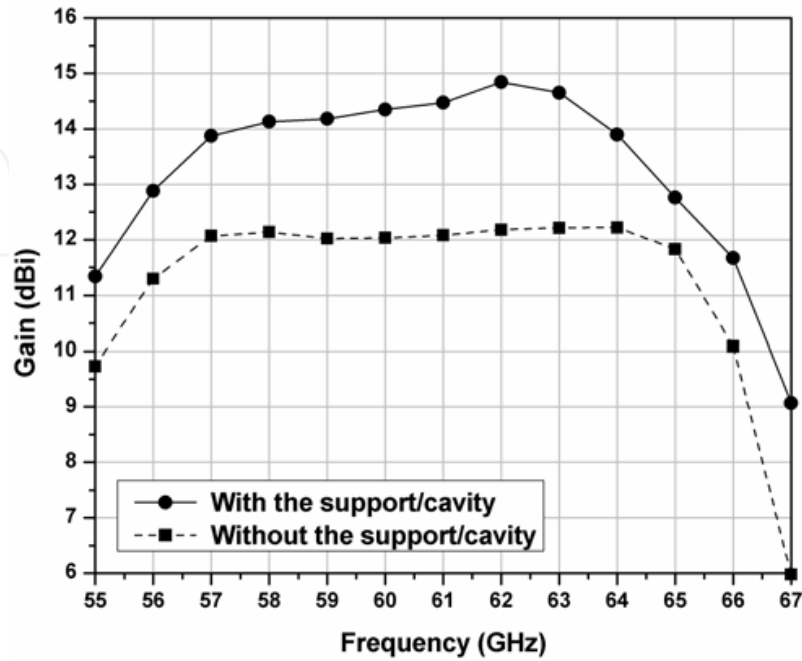

Fig. 16. Simulated gain of both configurations (with and without the brass support and cavity).
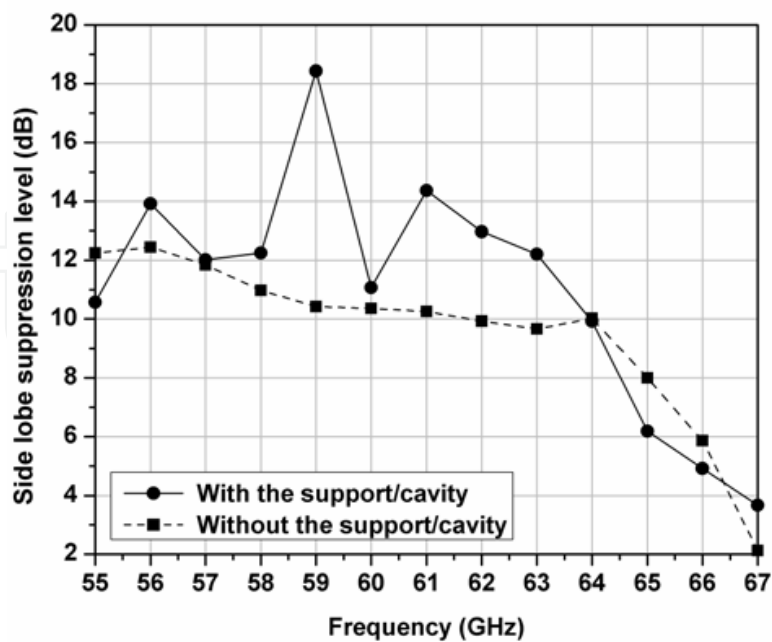

Fig. 17. Simulated side lobe suppression levels of both configurations (with and without the brass support and cavity).

The radiation patterns of both configurations near mid-band (61 GHz) are shown in Figure 18. The side lobe levels of the antenna fitted with the brass housing are clearly lower. Also note that the cross-polarized field levels are very low, especially the cross-polarized E-field, which is negligible (thus not visible in Figure 18).


E-plane (co)
H-plane (co)
H-plane (cross)

(a)   (b)
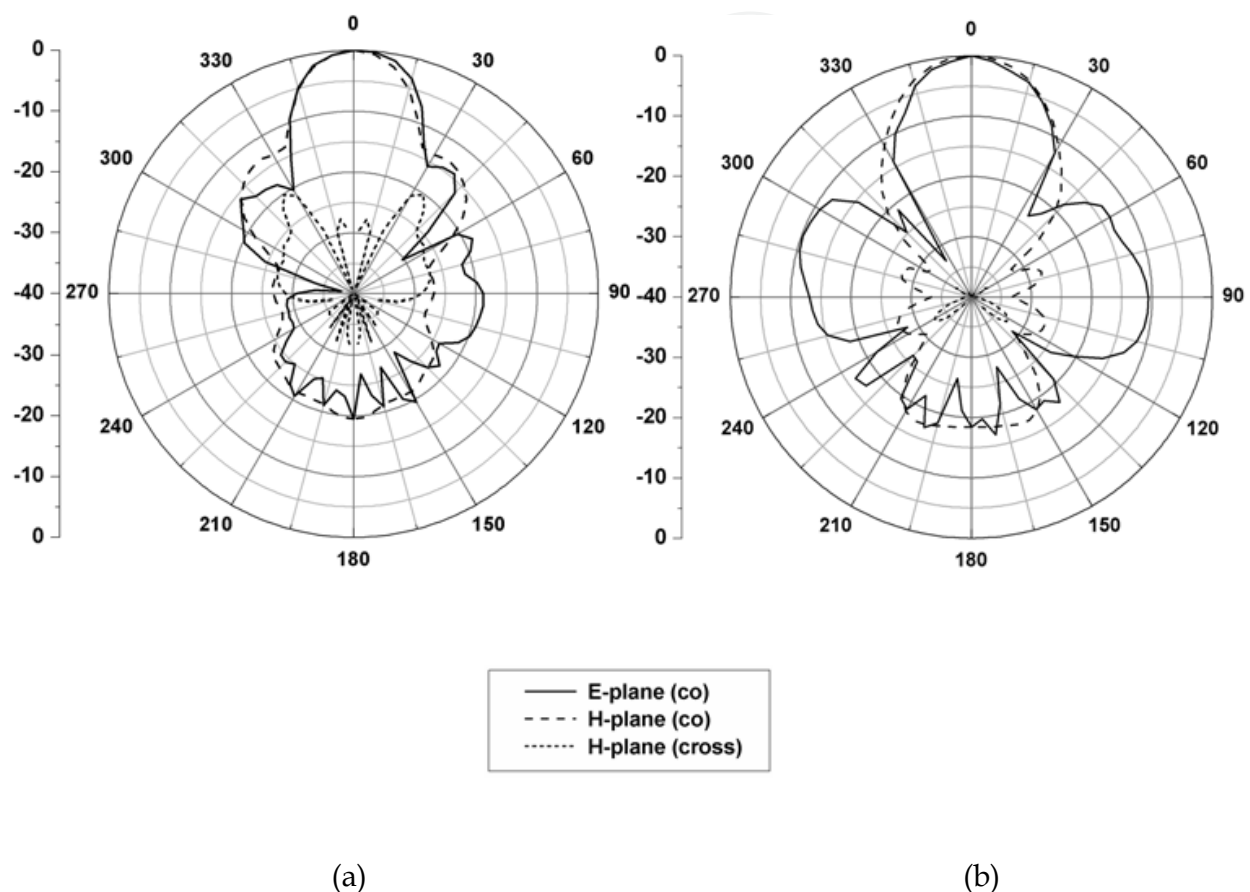
Fig. 18. Simulated normalized radiation patterns at 61 GHz: (a) with the brass support and cavity and (b) without the brass support and cavity.

4.3 Parametric study

The results of a short parametric study are presented in Figure 19. In Figure 19a, the radius (*r*) of the cavity is varied from 6.75 to 7.75 mm. In Figure 19b, the height (*h*) of the cavity is varied from 2.5 to 3.5 mm. From these results, it is obvious that gain is directly affected by the dimensions of the metallic cavity, especially its radius. By conducting similar studies for the side lobe levels and impedance bandwidth, it is possible to optimize the cavity and reach the best side lobe suppression/gain/bandwidth tradeoff.

4.4 Discussion

In this section, a new modified geometry for a hybrid microstrip/dielectric resonator antenna has been presented. The simulated gain remains over 14 dB for a large portion of the 10 GHz impedance bandwidth. The side lobe levels are also significantly lowered with the addition of a metallic cavity.
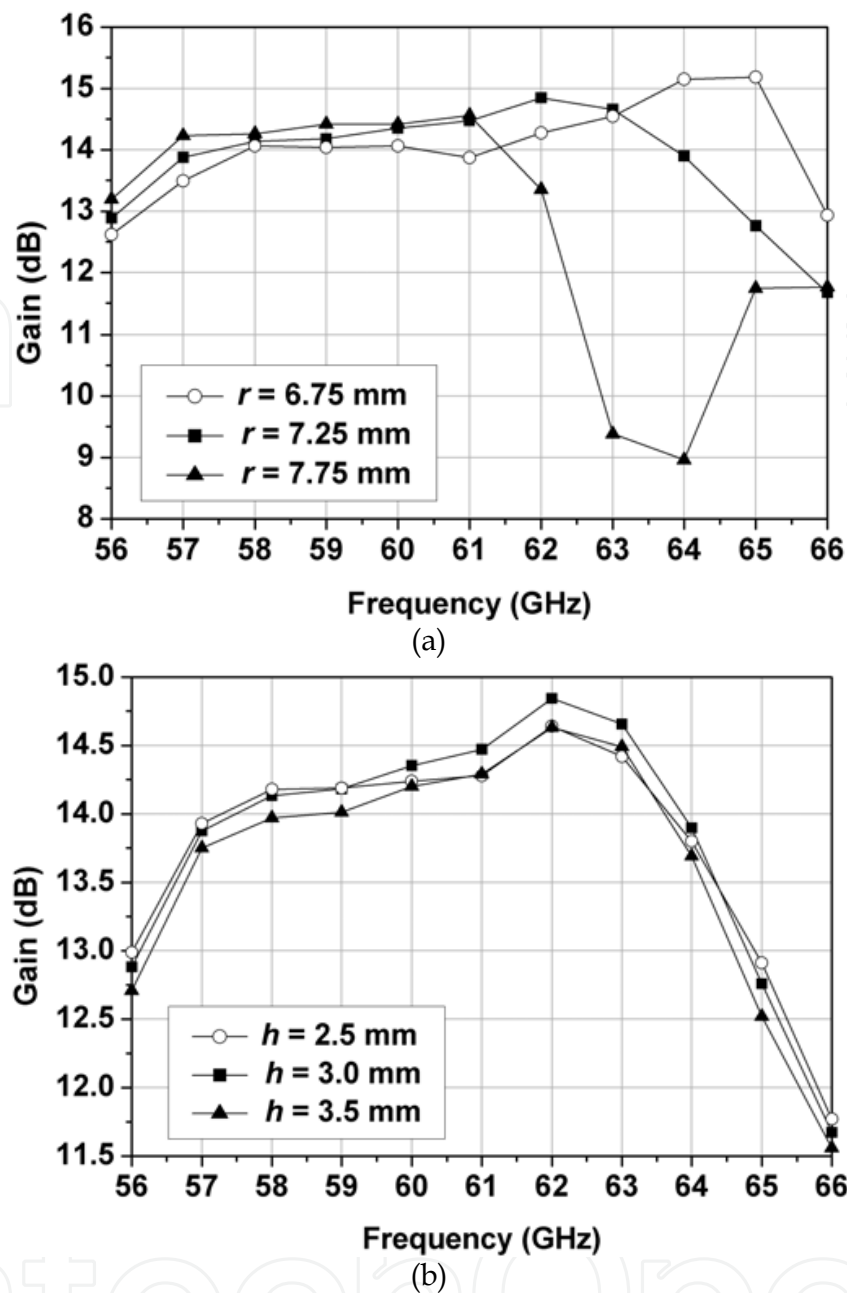
Fig. 19. Parametric study: (a) radius of the cavity and (b) height of the cavity.

5. Conclusion

In this chapter, two hybrid microstrip antennas were briefly introduced. In each case, it was possible to enlarge the impedance bandwidth and increase the electrical size (thus enhancing the gain) of the antenna by using two different radiating elements (a microstrip patch and a dielectric resonator). These examples show how hybrid antennas can be used to meet various requirements and still remain relatively easy to design and manufacture.

In addition to fabricating prototypes based on the improved antenna geometry of Section 4, other projects could be undertaken in the future. Initially, an optimization campaign would probably help to limit the losses generated by the 1.85 mm connector (by improving the coaxial-to-microstrip transition). Indeed, though this stage is not absolutely necessary, that

would facilitate the performance evaluation of the antennas. Finally, within the framework of a project of greater scale, it would be possible to integrate various active components (a low noise amplifier, for example) on the feed side (with the microstrip line), to design a compact antenna front-end. The metallic support could then cover the back of the antenna and protect these components. The dimensions of this protective cover could even be optimized to reduce the undesired backward radiation of the antenna.

6. References

Balanis, C. A. (2005) *Antenna Theory: Analysis and Design*, 3rd ed. Hoboken, NJ: Wiley-Interscience.

Cohn, S. B. (1968) Microwave bandpass filters containing high-Q dielectric resonators. *IEEE Transactions on Microwave Theory and Techniques*, Vol. 16, No. 4, pp. 218-227.

Esselle, K. P. & Bird, T. S. (2005). A Hybrid-Resonator Antenna: Experimental Results. *IEEE Transactions on Antennas and Propagation*, Vol. 53, No. 2, pp. 870-871.

George, J.; Aanandan, C. K.; Mohanan, P.; Nair, K. G.; Sreemoolanathan, H. & Sebastian, M. T. (1998). Dielectric-resonator-loaded microstrip antenna for enhanced impedance bandwidth and efficiency. *Microwave and Optical Technology Letters*, Vol. 17, No. 3, pp. 205-207.

Horng, T.-S. & Alexopoulos, N. G. (1993). Corporate feed design for microstrip arrays. *IEEE Transactions on Antennas and Propagation*, Vol. 41, No. 12, pp. 1615-1624.

Huang, K. C. & Wang, Z. (2006). Millimeter-wave circular polarized beam-steering antenna array for gigabit wireless communications. *IEEE Transactions on Antennas and Propagation*, Vol. 54, No. 2, pp. 743-746.

Kajfez, D. & Guillon, P. (1986) *Dielectric Resonators*, Dedham, MA: Artech House, Inc.

Malherbe, J. A. G. (1989). Analysis of a linear antenna array including the effects of mutual coupling. *IEEE Transactions on Education*, Vol. 32, No. 1, pp. 29-34.

Mohammadian, A. H.; Martin, N. M. & Griffin, D. W. (1989). A theoretical and experimental study of mutual coupling in microstrip antenna arrays. *IEEE Transactions on Antennas and Propagation*, Vol. 37, No. 10, pp. 1217-1223.

Oh, J.; Baek, T.; Shin, D.; Rhee, J. & Nam, S. (2007). 60 GHz CPW-fed dielectric-resonator-above-patch (DRaP) antenna for broadband WLAN applications using micromachining technology. *Microwave and Optical Technology Letters*, Vol. 49, No. 8, pp. 1859-1861.

Perron, A., Talbi, L. & Denidni, T. A. (2007). Dual-polarised CPW-fed microstrip antenna for wireless applications at 2.45 GHz. *IEE Electronics Letters* Vol. 43, No. 14 (2007), 740-742.

Perron, A.; Denidni, T. A. & Sebak, A. R. (2009). High-gain hybrid dielectric resonator antenna for millimeter-wave applications: design and implementation. *IEEE Transactions on Antennas and Propagation*, Vol. 57, No. 10, pp. 2882-2892.

Porter, B. G., Rauth, L. L., Mura, J. R. & Gearhart, S. S. (1999). Dual-Polarized Slot-Coupled Patch Antennas on Duroid with Teflon Lenses for 76.5-GHz Automotive Radar Systems. *IEEE Transactions on Antennas and Propagation*, Vol. 47, No. 12, pp. 1836-1842.

Uchimura, H.; Shino, N. & Miyazato, K. (2005). Novel circular polarized antenna array substrates for 60GHz-band. *2005 IEEE MTT-S Digest*, p. 1875-1878, Long Beach, CA, June 2005.

Weily, A. R. & Guo, Y. G. (2009). Circularly polarized ellipse-loaded circular slot array for millimeter-wave for WPAN applications. *IEEE Transactions on Antennas and Propagation*, Vol. 57, No. 10, pp. 2862-2870.

Microstrip Antennas

Edited by Prof. Nasimuddin Nasimuddin

In the last 40 years, the microstrip antenna has been developed for many communication systems such as radars, sensors, wireless, satellite, broadcasting, ultra-wideband, radio frequency identifications (RFIDs), reader devices etc. The progress in modern wireless communication systems has dramatically increased the demand for microstrip antennas. In this book some recent advances in microstrip antennas are presented.

How to reference

In order to correctly reference this scholarly work, feel free to copy and paste the following:

INTECH
open science | open minds